Nanoscale

Accepted Manuscript

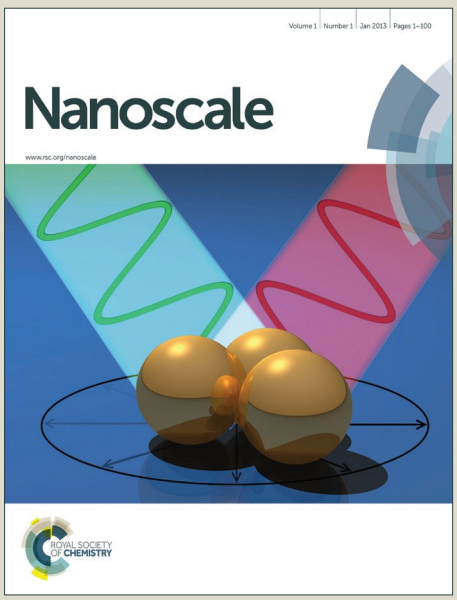

ROYAL SOCIETY OF CHEMISTRY

www.rsc.org/nanoscale

Nanoscale

COMMUNICATION

Charge Generation and Morphology in P3HT:PCBM Nanoparticles Prepared by Mini-emulsion and Reprecipitation Methods

Received 00th January 20xx,
Accepted 00th January 20xx

DOI: 10.1039/x0xx00000x

www.rsc.org/

Kyra N. Schwarz, Sam B. Farley, Trevor A. Smith and Kenneth P. Ghiggino*

Organic semiconductor nanoparticles provide a potentially scalable approach for photovoltaics that can be processed from aqueous media. Particles of poly(3-hexylthiophene) (P3HT):phenyl-C_{61}-butyric acid methyl ester (PCBM) were prepared using two techniques; those produced by a mini-emulsion method contained greater amounts of crystalline P3HT domains with charge generation resembling phase-separated annealed solvent-cast films.

A principal challenge for organic photovoltaics remains to transfer the technology from the laboratory to large-scale production.[1,2] Despite improvements in device performance driven largely by the development of new low band gap donor materials, there remains significant process performance dependency issues in controlling active layer nanomorphology across large device areas.[3,4] This control is necessary to effectively translate efficiencies from the laboratory to the production line. The use of significant volumes of toxic chlorinated solvents also presents barriers for high-speed industrial printing development.

In recent years, approaches to processing using low toxicity, eco-friendly solvents have been making significant progress. Due to the traditional solubility limitations of organic semiconductors, the development of soluble analogues using side-chain modification can provide options for improved processability.[5] Alternatively, nanoparticle suspensions of active-layer materials in water or alcohol have gained increasing attention and allow the use of existing, well-developed hydrophobic donors and acceptors.[6-10] Despite a modest beginning, composite donor-acceptor organic nanoparticle processed photovoltaic devices have recently made noteworthy improvements with the efficiency of a poly(3-hexylthiophene) (P3HT):indene-C60 bisadduct (ICBA) device reaching over 4%,[10] comparable to the photoconversion efficiencies of 4-6% for similar bulk heterojunction devices cast directly from chlorinated solvents.[11]

Bulk heterojunction morphology can be influenced and tuned during the nanoparticle preparation process and pr aggregation of the donor and acceptor domains has been shown to persist throughout processing.[3] Hence the development of nanoscale morphology, which is of ke importance to performance, can be somewhat decoupled from the specific coating operation, and the distribution of dono and acceptor can be fixed prior to deposition. Using this strategy, it is possible to optimise the intrinsic characteris of a given nanoparticle formulation for the best photovolta performance and then optimise the coating process to yield set of extrinsic film properties.[4]

There are two main approaches to prepare composit donor-acceptor nanoparticles; the surfactant-based mini emulsion method, and the additive-free reprecipitatio method. The mini-emulsion approach uses surfactant and sonication to produce a dispersion of stable nanoparticles the range of 30 nm to 500 nm depending on surfactant concentration.[12] Mini-emulsion nanoparticles of conjuga d polymer and fullerene-based acceptors typically adopt a core-shell type distribution during formation, confirmed using scanning transmission X-ray microscopy[3,13] and small ang neutron scattering,[4] with corresponding bulk heterojunction devices reaching photo-conversion efficiencies (PCE) of 2.5%. The reprecipitation approach requires the organ semiconductor to be dissolved in a good solvent and then quickly injected into a poor solvent, which is being rapid stirred.[8] Nanoparticles can range in diameter from 5 nm to 400 nm and devices made using this method have reached PCEs o 4.1% (P3HT:ICBA in methanol), although after deposition, nanoparticle films were subjected to high-temperatur annealing.[10] It has been demonstrated that by manipulating the processing conditions of these nanoparticles, is it possibl to form a wide variety of different structures, with a divers range of internal structural and morphological heterogeneity.[4]

The chain conformation of organic semiconductin polymers has a significant impact on device performance, and the relationship between morphology and performance in bul

School of Chemistry, University of Melbourne, Victoria, 3010, Australia. E-mail: ghiggino@unimelb.edu.au
Electronic Supplementary Information (ESI) available: See DOI: 10.1039/x0xx00000x

heterojunction organic solar cells has been studied extensively over the past decade.[14-16] Upon film formation or aggregation, regioregular P3HT can self-assemble into 2D π-stacked lamellar structures, which can result in a significant improvement in charge mobility,[17] and charge photogeneration when accompanied by intermixed regions.[15,18]

In order to realise efficient nanoparticle devices, it is necessary to understand how a composite particle's internal morphology contributes to photocurrent generation. In this paper we employ steady-state absorption and sub-picosecond transient absorption (TA) spectroscopy to probe the effect of nanoparticle preparation on charge generation dynamics and P3HT H-aggregate character, comparing features for particles produced by the mini-emulsion and reprecipitation methods. Previous spectroscopic and morphological investigations of P3HT:PCBM reprecipitation nanoparticles have used steady-state and single molecule fluorescence studies to determine morphological changes with different acceptor concentration.[19-21] The ultrafast dynamics of reprecipitation particles have been examined by Kee et al.,[22,23] and have demonstrated the presence of excited-state and charge separated species for different acceptor concentrations. We present a direct assessment of particle types of comparable size and donor-acceptor fractional composition and provide an interpretation of differences in blend morphology and charge generation.

Fig. 1a indicates the structure of 1:1 P3HT:PCBM blend nanoparticles prepared by the mini-emulsion and reprecipitation methods, with Fig. 1b showing the respective absorption spectra of nanoparticle suspensions where particles are a comparable size. The absorption closely resembles that of P3HT:PCBM thin films, with the P3HT region (400-650 nm) consisting of two components; a higher energy region dominated by contributions from disordered chains, and a lower energy region attributed to crystalline P3HT that arises due to weakly interacting H-aggregate states formed in self-assembled 2D π-stacked lamellar structures. Absorption and emission of P3HT-only nanoparticles share the same features and can be found in the ESI (Fig. S1). The vibronic structure is more prominent in the mini-emulsion nanoparticle spectrum indicated by shoulders at 610 nm and 556 nm that correspond to the 0-0 and 0-1 transitions within P3HT aggregates.[24] The nanoparticle fabrication process results in aggregates that exhibit features similar to thermally or solvent annealed bulk heterojunction films of these materials, despite the lack of any elevated temperature processing.[3,22] Nanoparticle structure is largely maintained through the construction of nanoparticle OPV devices,[3] possessing a "preordered" active layer film structure depending on colloidal preparation conditions.

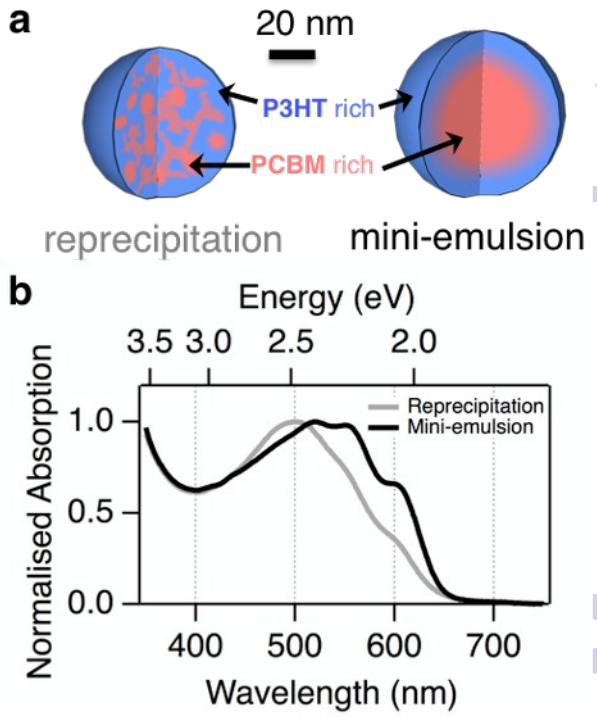

Fig. 1. a) Schematic of P3HT:PCBM blend nanoparticle structure and b) normalised absorption spectra of P3HT:PCBM 1:1 blend nanoparticles in water prepared by the reprecipitation (grey) and mini-emulsion (black) methods.

An established analytical model of weakly interacting H-aggregates (excitonic coupling) by Spano allows for a quantitative analysis of the polymer aggregate species, and consequently, the morphology of P3HT using linear absorption spectroscopy.[24,25] We note that Spano and Silva have more recently extended on the H-aggregate model for P3HT to include a description both of H- and J-aggregate behaviour where the latter can occur under exceptional processing conditions.[26] However, they show that in the majority of cases the H-aggregate model remains quite accurate for predicting the absorption spectral line shape. To confirm that these nanoparticle systems fall clearly within the H-aggregate regime we also referred to Hellmann et al.[27] who monitor P3HT absorption spectra features in a system that transitions from H- to mainly J-aggregate behaviour.

The H-aggregate model involves dissecting the vibronic progression and providing quantitative estimates of the aggregate free exciton bandwidth, W, and in turn the crystalline quality. The model describes the aggregate region of the absorption spectrum using a series of Gaussian bands, with further details available in the ESI.

Using the ratio of the intensities of the 0-0 ($A_{0\text{-}0}$) and 0-1 ($A_{0\text{-}1}$) transitions extracted from the fit, the free exciton bandwidth, W, can be estimated using Equation 1:

$$\frac{A_{0-0}}{A_{0-1}} \approx \left(\frac{1-0.24W/E_p}{1+0.073W/E_p}\right)^2 \qquad (1)$$

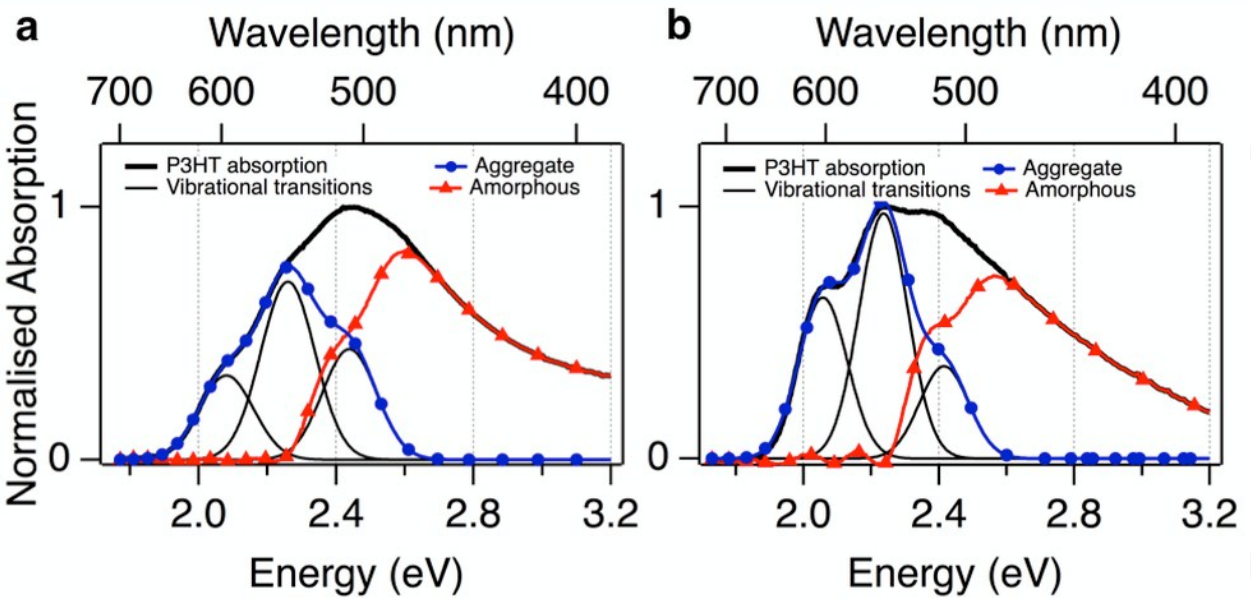

Fig. 2. Absorption spectra of the P3HT component (thick black line) of a) reprecipitation and b) mini-emulsion 1:1 P3HT:PCBM blend nanoparticle preparations. Best fits for the aggregate component of the spectra using equation 1 are shown (thin black lines showing the vibrational transitions) with the sum (dashed blue) and subtracted (dashed red) to indicate contributions of the aggregate and amorphous, respectively. The aggregate region consists of the best fit of the low energy absorption region from 1.9 - 2.25 eV (550 – 650 nm). The amorphous region is the result of the subtraction of the aggregate region from the total P3HT absorption.

where E_p is the energy of the main intramolecular vibration. The free exciton bandwidth is related to intrachain order and inversely related to conjugation length. The absorption spectrum of P3HT within the P3HT:PCBM blend nanoparticles was generated by subtracting a normalised spectrum of PCBM prior to analysis, using the method of Turner et al.[28]

Fig. 2 illustrates the absorption spectra and P3HT vibronic structure best fits obtained using equation S1 (see ESI) for (a) reprecipitation and (b) mini-emulsion blend nanoparticle suspensions. The free exciton bandwidth, W, for blend nanoparticles in solution was determined as 194 meV for the reprecipitation type, comparable to 197 meV reported by Turner et. al.,[28] for P3HT:PCBM unannealed blend films cast from chloroform. These values are indicative of larger free exciton bandwidths, and therefore shorter average conjugation lengths and lower crystalline quality. In contrast, mini-emulsion nanoparticles gave a free exciton bandwidth of 114 meV, which can be compared to 160 °C annealed films cast from chloroform and dichlorobenzene, which exhibit values of 135 meV and 92 meV respectively.[28] These lower values of W are indicative of higher crystalline quality and larger conjugation lengths relative to the reprecipitation type particles.

The proportion of the nanoparticle consisting of aggregates can also be determined using the fraction of absorption spectra assigned to aggregate absorption,[29,30] and the relative increase in oscillator strength when a polymer chain goes from twisted amorphous to planar aggregated.[31] Reprecipitation nanoparticles were determined to have ca. 45% of the P3HT component as aggregated material, whereas mini-emulsion blend particles have ca. 57% aggregated P3HT phase. This adds to present morphological information on the structure of mini-emulsion nanoparticles that are reported to have an 80% pure PCBM core surrounded by a P3HT shell.[3]

Morphology with a low degree of intra- and inter-chain disorder has been linked to an increase in hole mobility and a concurrent overall improvement in charge carrier generation and extraction efficiency in P3HT:PCBM photovoltaic devices.[15] This indicates that the mini-emulsion particles, with larger average P3HT conjugation lengths and a greater average crystalline component compared to the reprecipitation particles, should present a favourable nanoscale morphology despite the lack of high boiling-point solvents or elevated temperature processing.

Transient absorption spectra and dynamics of P3HT:PCBM blend nanoparticles are shown in Fig. 3, for (a) reprecipitation and (b) mini-emulsion suspensions in water. The negative signal between 500-620 nm represents the ground-state depletion, occurring in the same region as the steady-state absorption signal. The depletion signals in both nanoparticle types are long lasting, particularly in the mini-emulsion sample, indicative of the formation of a long-lived species. This is in contrast to neat P3HT nanoparticles, where both preparation types exhibit a ground-state depletion, which almost entirely recovers within the experimental time frame of 750 ps, indicating that excitons have returned to the ground state, consistent with a P3HT exciton lifetime of ~200 ps.[3] Negative-going peaks at 565 nm and 620 nm which represent the 0-1 and 0-0 vibronic progressions, respectively, are present in the mini-emulsion blend and also clearly visible in neat P3HT nanoparticles of both preparation types (see Fig. S2, ESI). The mini-emulsion preparation of P3HT:PCBM blend nanoparticles (Fig. 3b) exhibits a much more structured ground state bleach than the reprecipitation nanoparticles (Fig. 3a), indicating that

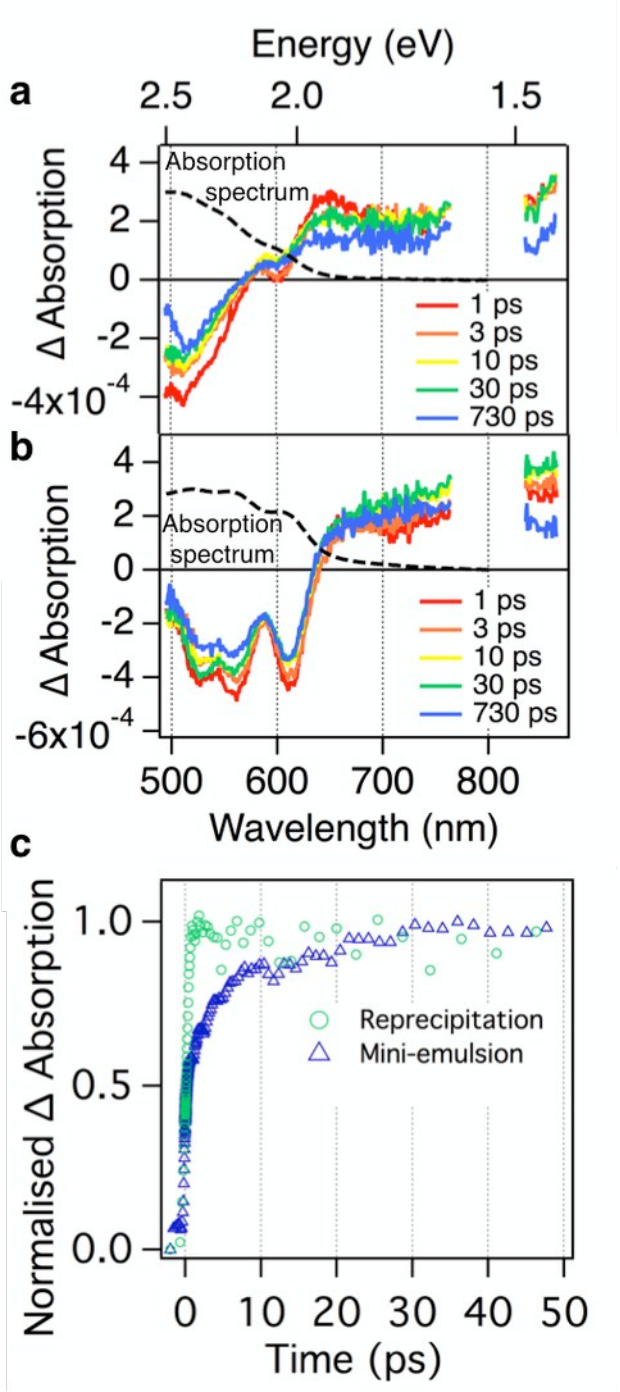

Fig. 3. P3HT:PCBM blend nanoparticle transient absorption spectra of suspensions prepared using a) the reprecipitation and b) the miniemulsion methods, with c) showing the kinetics at 690 nm for both samples. Steady-state absorption spectra are shown in a) and b) (black dotted line), and pump fluence at 400 nm was 9.75 μJ/cm^2.

in the former, excitations and long-lived species preferentially occupy the planarised H-aggregate P3HT regions rather than the amorphous polymer.[33] This also indicates, in contrast to the reprecipitation method, that the PCBM in mini-emulsion particles has not significantly disrupted the P3HT chain planarity and lamellar structure that is observed in both varieties of neat P3HT nanoparticle.

A broad positive signal from 680-900 nm (limited by the probe pulse range) has been previously attributed[33-36] to the photo-induced absorption of the P3HT hole polaron, the product of charge transfer. This broad photo-induced absorption was similarly observed in ultrafast transient absorption spectroscopy performed by Kee et al.,[22] in P3HT:PCBM reprecipitation nanoparticles, in the near-infrared region, peaking at 1000 nm and also attributed to P3HT polarons. This signal is present in both samples at times < 100 fs after excitation, and in addition, the mini-emulsion sample also exhibits a further grow-in of this photoinduced absorption, with kinetic traces at 690 nm shown in Fig. 3c. The rise in the mini-emulsion particle polaron signal is complete within ~30 ps and is indicative of excitons generated in the P3HT phase that diffuse to an interfacial or intermixed region and then dissociate.[33,37] These spectroscopic dynamics are similar to that of annealed P3HT:PCBM blend films, indicating that excitons formed in the polymer phase must diffuse in order to be quenched, as shown by Friend and coworkers.[33] This rise can be obscured by high pump excitation fluences which can result in exciton-exciton or exciton-charge annihilation,[38,39] as shown in Fig. S3 (see ESI). In contrast, the hole polaron population for the reprecipitation particles peaks at earlier times, consistent with finer phase separation indicating that excitons do not need to diffuse to reach a donor acceptor interface. This is similarly observed for unannealed P3HT:PCBM blend films shown in other work.[33,36]

Annealing in P3HT:PCBM blend films has been shown to be advantageous to charge generation due to phase separation and the formation of ordered crystalline domains in both polymer and fullerene, allowing effective charge separation and a reduction in geminate recombination.[36,40] The similarities in the charge generation dynamics of P3HT:PCBM mini-emulsion nanoparticles to annealed blend films of the same materials suggest that they too have a structure favourable for reducing geminate recombination. However, nanoparticles have further structural factors to consider such as the presence of surfactant and the particle's core-shell structure.

Venkataraman et. al., have recently demonstrated that surfactants present in mini-emulsion blend devices do not significantly impede charge transport,[41] provided that the excess surfactant is removed during particle preparation. Other work suggests that the donor-rich shell makes it more difficult for photogenerated electrons to be transported out of the particle, leading to higher rates of internal recombination and subsequently lower measured photocurrents and device performance.[4] This highlights the importance of understanding how the size and internal distribution of materials affect device performance. However, by manipulating processing conditions, it is possible to form variations on the typical core shell composition.[4,42] Pozzo and coworkers have shown that the best performing composite mini-emulsion nanoparticles are those that have a uniform distribution of conjugated polymer and fullerene throughout the nanoparticle volume such that electrons and holes are easily transported out of the particle.[4] An alternative approach is to introduce processing

variations that can assist in making reprecipitation type nanoparticles more crystalline, rather than relying on elevated temperature processing after nanoparticle deposition.

Conclusions

In this work steady-state and sub-picosecond transient absorption spectroscopy has been applied to compare the morphology and excited state processes in P3HT:PCBM nanoparticles prepared by both mini-emulsion and reprecipitation methods. The absorption spectrum can be used as a simple indicator of excitonic coupling, intrachain order and the fraction of crystalline regions within the samples, where the mini-emulsion (reprecipitation) method gives a free exciton bandwidth of 114 meV (197 meV) and proportion of crystalline P3HT as 57 % (45 %).

Charge photogeneration, probed by transient absorption spectroscopy, was observed in both nanoparticle types, indicating that nanoparticles produced by the mini-emulsion (reprecipitation) technique have charge generation dynamics that more closely resemble annealed (unannealed) solvent cast films than do the reprecipitation-based particles. The mini-emulsion particles have a population of P3HT excitons that diffuse to the interface over a period of ~30 ps and morphology consistent with one where geminate recombination is suppressed. Despite favourable charge separation properties, which do not require elevated temperature thermal treatment, the typical core-shell structure may inhibit efficient charge collection in devices fabricated from mini-emulsion type particles.

This research provides a deeper insight into the role of morphology on charge photogeneration in organic semiconductor donor-acceptor blend nanoparticles that is relevant to their potential application in organic photovoltaic materials and other organic optoelectronic devices.

Experimental section

Nanoparticle preparation

Aqueous nanoparticle dispersions of 50 kDa regioregular poly(3-hexylthiophene) (Merck) and phenyl-C61-butyric acid methyl ester (PCBM, technical grade, 99%, Solenne BV) were prepared in 18.2 MΩ MilliQ water (Millipore Simplicity system).

Reprecipitation nanoparticles were prepared using 1 mg of a 1:1 P3HT:PCBM w/w mixture dissolved in 1 ml of tetrahydrofuran (THF), (Sigma-Aldrich, Chromasolv® inhibitor-free) and stirred for 20 minutes at 40°C. The THF solution was transferred to a syringe and rapidly injected into 8 ml of MilliQ water under vigorous agitation and remaining THF was removed under reduced pressure and filtered (0.45 µm PES filter) before characterisation.

Mini-emulsion nanoparticles were prepared using 60 mg of a 1:1 P3HT:PCBM w/w mixture dissolved in 1.12 mL chloroform (Sigma-Aldrich, Chromasolv® inhibitor-free) and stirred for 20 minutes at 40°C. The solution was sonicated (Unisonics FHP12DH) for 10 minutes and stirred again for 10 minutes at 40°C, then added to a 42 mM aqueous sodium dodecylsulfate (SDS, Scharlau, 95% extra-pure) solution and stirred rapidly at 40°C for 1 hour to form a macroemulsion. The macroemulsion was sonicated (Branson S450D) with a 5 mm tapered microtip for 2 minutes at 60 % amplitude in pulse mode (0.5 s on, 1 s off). The subsequent mini-emulsion was then slowly heated to 60 °C while stirring for 3 hours to evaporate the chloroform and centrifuged at 18,000 rpm for 16 minutes to concentrate the dispersion and remove excess surfactant (Sartorius Ultrafiltration centrifuge tube). Dispersions were filtered through a 0.2 µm PES syringe filter before undergoing their final ultracentrifuge cycle.

Nanoparticle Characterisation

Particle size and polydispersity index, (PDI) were determined by dynamic light scattering (DLS) using a Zetasizer Nano-ZS (Malvern Instruments). Nanoparticles produced by the two methods had similar average particle sizes; the mini-emulsion particles with average hydrodynamic diameters of 84 nm (P3HT) and 110 nm (blend), and the reprecipitation particles having diameters of 92 nm (P3HT) and 79 nm (blend). The PDI for all particle types was 0.23 ± 0.03.

Absorption and fluorescence spectra were recorded using a Varian Cary 50 UV-Vis spectrophotometer and Varian Eclipse spectrofluorimeter respectively, in a 10 mm quartz cuvette. Fluorescence spectra were recorded using an excitation wavelength of 450 nm, where optical densities of solutions were kept below 0.1 at the excitation wavelength to minimise reabsorption effects.

Sub-picosecond transient absorption

The broadband picosecond transient absorption setup is described in detail elsewhere.[43] The pump beam (400 nm) was attenuated to a pulse power of 46 nJ/pulse and a spot diameter of 0.8 mm was used to give an excitation density of 9.75 µJ/cm^2, to reduce artifacts associated with exciton-exciton[44] and exciton-charge annihilation.[38,39] The relative orientation of pump and probe polarisation was 54.7° and all spectra were corrected for the chirp of the supercontinuum probe.

Acknowledgements

This work was made possible by support from the Australian Renewable Energy Agency, which funds the project grants within the Australian Centre for Advanced Photovoltaics. K.N.S. acknowledges the Australian Renewable Energy Agency for a postgraduate scholarship. Responsibility for the views, information or advice herein is not accepted by the Australian Government.

Notes and references

1 L. Dou, J. You, Z. Hong, Z. Xu, G. Li, R. A. Street and Y. Yang, *Adv. Mater.*, 2013, **25**, 6642–6671.

2 R. R. Søndergaard, M. Hösel and F. C. Krebs, *J. Polym. Sci. Part B: Polym. Phys.*, 2012, **51**, 16–34.
3 S. Ulum, N. Holmes, D. Darwis, K. Burke, A. L. D. Kilcoyne, X. Zhou, W. Belcher and P. Dastoor, *Sol. Energ. Mat. and Sol. C.*, 2013, **110**, 43–48.
4 J. J. Richards, C. L. Whittle, G. Shao and L. D. Pozzo, *ACS Nano*, 2014, **8**, 4313–4324.
5 C. Duan, K. Zhang, C. Zhong, F. Huang and Y. Cao, *Chem. Soc. Rev.*, 2013, **42**, 9071.
6 K. Landfester, R. Montenegro, U. Scherf, R. Guntner, U. Asawapirom, S. Patil, D. Neher and T. Kietzke, *Adv. Mater.*, 2002, **14**, 651–655.
7 T. Kietzke, D. Neher, K. Landfester, R. Montenegro, R. Güntner and U. Scherf, *Nature Materials*, 2003, **2**, 408–412.
8 C. Szymanski, C. Wu, J. Hooper, M. A. Salazar, A. Perdomo, A. Dukes and J. McNeill, *J. Phys. Chem. B*, 2005, **109**, 8543–8546.
9 T. R. Andersen, T. T. Larsen-Olsen, B. Andreasen, A. P. L. Böttiger, J. E. Carlé, M. Helgesen, E. Bundgaard, K. Norrman, J. W. Andreasen, M. Jørgensen and F. C. Krebs, *ACS Nano*, 2011, **5**, 4188–4196.
10 S. Gärtner, M. Christmann, S. Sankaran, H. Röhm, E. Prinz, F. Penth, A. Pütz, A. E. Türeli, B. Penth, B. Baumstümmler and A. Colsmann, *Adv. Mater.*, 2014, **26**, 6653–6657.
11 M. T. Dang, L. Hirsch and G. Wantz, *Adv. Mater.*, 2011.
12 J. Pecher and S. Mecking, *Chem. Rev.*, 2010, **110**, 6260–6279.
13 K. B. Burke, A. J. Stapleton, B. Vaughan, X. Zhou, A. L. D. Kilcoyne, W. J. Belcher and P. C. Dastoor, *Nanotechnology*, 2011, **22**, 265710.
14 C. J. Brabec, M. Heeney, I. McCulloch and J. Nelson, *Chem. Soc. Rev.*, 2011, **40**, 1185.
15 K. Vandewal, S. Himmelberger and A. Salleo, *Macromolecules*, 2013, **46**, 6379–6387.
16 I. Botiz and N. Stingelin, *Materials*, 2014, **7**, 2273–2300.
17 J. F. Chang, B. Sun, D. W. Breiby, M. M. Nielsen, T. I. Sölling, M. Giles, I. McCulloch and H. Sirringhaus, *Chem. Mat.*, 2004, **16**, 4772–4776.
18 S. V. Kesava, Z. Fei, A. D. Rimshaw and C. Wang, *Adv. En. Mat.*, 2014, 1400116.
19 Z. Hu and A. J. Gesquiere, *Chem. Phys. Lett.*, 2009, **476**, 51–55.
20 Z. Hu, D. Tenery, M. S. Bonner and A. J. Gesquiere, *J. Lum.*, 2010, **130**, 771–780.
21 A. M. Crotty, A. N. Gizzi, H. J. Rivera-Jacquez, A. E. Masunov, Z. Hu, J. A. Geldmeier and A. J. Gesquiere, *J. Phys. Chem. C*, 2014, **118**, 19975–19984.
22 S. N. Clafton, D. M. Huang, W. R. Massey and T. W. Kee, *J. Phys. Chem. B*, 2013, **117**, 4626–4633.
23 Y. Song, S. N. Clafton, R. D. Pensack, T. W. Kee and G. D. Scholes, *Nat Commun*, 2014, **5**, 1–7.
24 J. Clark, C. Silva, R. Friend and F. Spano, *Phys. Rev. Lett.*, 2007, **98**, 206406.
25 F. C. Spano, *J. Chem. Phys.*, 2005, **122**, 234701.
26 F. C. Spano and C. Silva, *Annu. Rev. Phys. Chem.*, 2014, **65**, 477–500.
27 C. Hellmann, F. Paquin, N. D. Treat, A. Bruno, L. X. Reynolds, S. A. Haque, P. N. Stavrinou, C. Silva and N. Stingelin, *Adv. Mater.*, 2013, **25**, 4906–4911.
28 S. T. Turner, P. Pingel, R. Steyrleuthner, E. J. W. Crossland, S. Ludwigs and D. Neher, *Adv. Funct. Mater.*, 2011, **21**, 4640–4652.
29 S. Berson, R. De Bettignies, S. Bailly and S. Guillerez, *Adv. Funct. Mater.*, 2007, **17**, 1377–1384.
30 A. J. Moulé and K. Meerholz, *Adv. Mater.*, 2008, **20**, 240–245.
31 J. Clark, J. F. Chang, F. C. Spano, R. H. Friend and C. Silva, *Appl. Phys. Lett.*, 2009, **94**, 163306.
32 J. Piris, T. E. Dykstra, A. A. Bakulin, P. H. M. V. Loosdrecht, W. Knulst, M. T. Trinh, J. M. Schins and L. D. A. Siebbeles, *J. Phys. Chem. C*, 2009, **113**, 14500–14506.
33 R. A. Marsh, J. M. Hodgkiss, S. Albert-Seifried and R. H. Friend, *Nano Lett.*, 2010, **10**, 923–930.
34 R. Osterbacka, C. P. An, X. M. Jiang and Z. V. Vardeny, *Science*, 2000, **287**, 839–842.
35 J. Guo, H. Ohkita, H. Benten and S. Ito, *J. Am. Chem. Soc.*, 2010, **132**, 6154–6164.
36 I. A. Howard, R. Mauer, M. Meister and F. Laquai, *J. Am. Chem. Soc.*, 2010, **132**, 14866–14876.
37 H. Yan, Y. Song, G. R. McKeown, G. D. Scholes and D. S. Seferos, *Adv. Mater.*, 2015, **27**, 3484–3491.
38 A. J. Ferguson, N. Kopidakis, S. E. Shaheen and G. Rumbles, *J. Phys. Chem. C*, 2008, **112**, 9865–9871.
39 J. M. Hodgkiss, S. Albert-Seifried, A. Rao, A. J. Barker, A. R. Campbell, R. A. Marsh and R. H. Friend, *Adv. Funct. Mater.*, 2012, **22**, 1567–1577.
40 P. E. Keivanidis, T. M. Clarke, S. Lilliu, T. Agostinelli, J. E. Macdonald, J. R. Durrant, D. D. C. Bradley and J. Nelson, *J. Phys. Chem. Lett.*, 2010, **1**, 734–738.
41 M. Bag, T. S. Gehan, D. D. Algaier, F. Liu, G. Nagarjuna, P. M. Lahti, T. P. Russell and D. Venkataraman, *Adv. Mater.*, 2013, **25**, 6411–6415.
42 S. Chambon, C. Schatz, V. Sébire, B. Pavageau, G. Wantz and L. Hirsch, *Mater. Horiz.*, 2014, **1**, 431–8.
43 K. P. Ghiggino, N. K. Giri, J. Hanrieder, J. D. Martell, J. Müller M. F. Paige, B. Robotham, J. Szmytkowski and R. P. Steer, *J. Phys. Chem. A*, 2013, **117**, 7833–7840.
44 M. A. Stevens, C. Silva, D. M. Russell and R. H. Friend, *Phys. Rev., B Condens. Matter*, 2001, **63**, 165213–18.